Supplementary Materials

Hierarchical $Cu(OH)_2$ Nanograsses-Decorated Bimetallic Nanoporous Glucose Sensor with Ultra-Low Detection Limit

Ao Zhang[a,b], Meng Liu[b,c], Xiangrui Feng[b,c], Shuo Liu[c], Yongzheng Zhang[c], Jinbiao Huang[d], Jiang Ma[d], Kailing Zhou[a,*], Jingbing Liu[a], Zhen Lu[b,e,*], Hao Wang[a]

[a]College of Materials Science and Engineering, Beijing University of Technology, Beijing 100124, China.

[b]Institute of Physics, Chinese Academy of Sciences, Beijing 100190, China.

[c]School of Physics and Physical Engineering, Qufu Normal University, Qufu 273165, China.

[d]College of Mechatronics and Control Engineering, Shenzhen University, Shenzhen, 518060, China.

[e]School of Physical Sciences, University of Chinese Academy of Sciences, Beijing 100049, China.

Corresponding authors.

E-mail addresses: zkling@bjut.edu.cn (K. Zhou), zhenlu@iphy.ac.cn (Z. Lu).

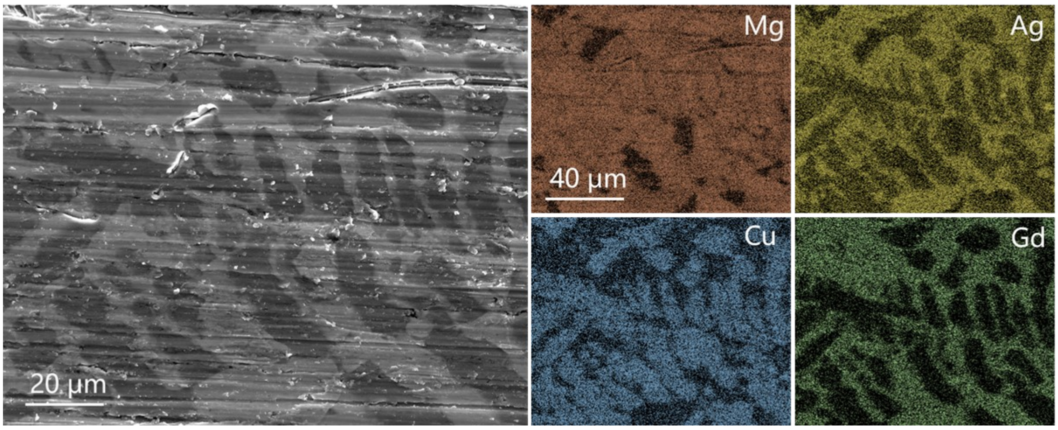

Figure S1. SEM image and corresponding EDS elemental mappings of $Mg_{54}Cu_{26.5}Ag_{8.5}Gd_{11}$ crystalline ingot.

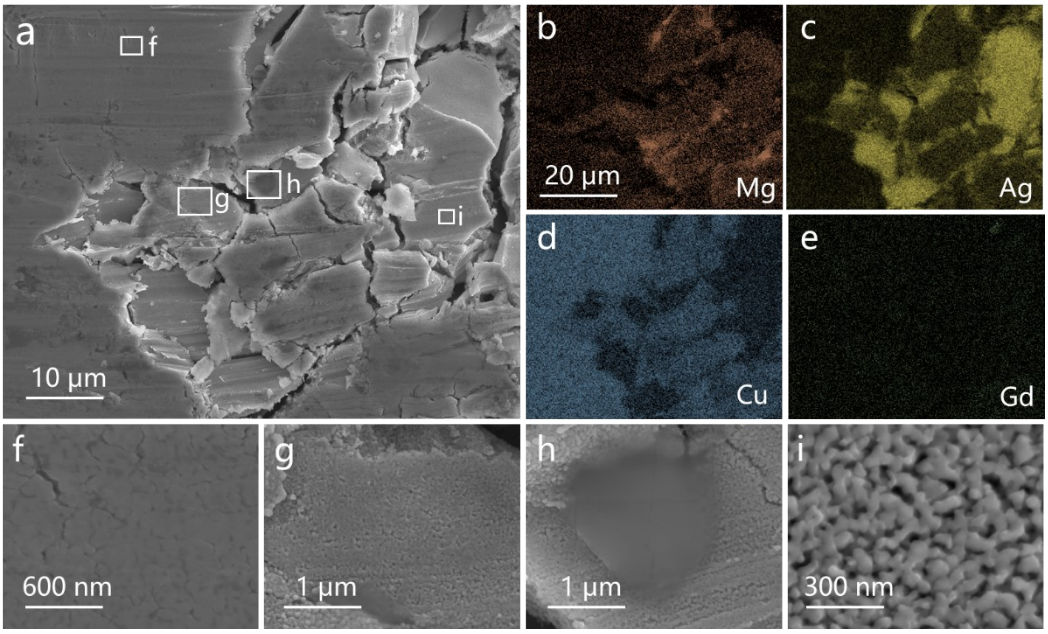

Figure S2. (a)-(e) SEM image and corresponding EDS elemental mappings of $Mg_{54}Cu_{26.5}Ag_{8.5}Gd_{11}$ crystalline ingot after dealloying at the same deallying condition of MG ribbons. (f)-(i) Magnified SEM images of four representative regions in (a).

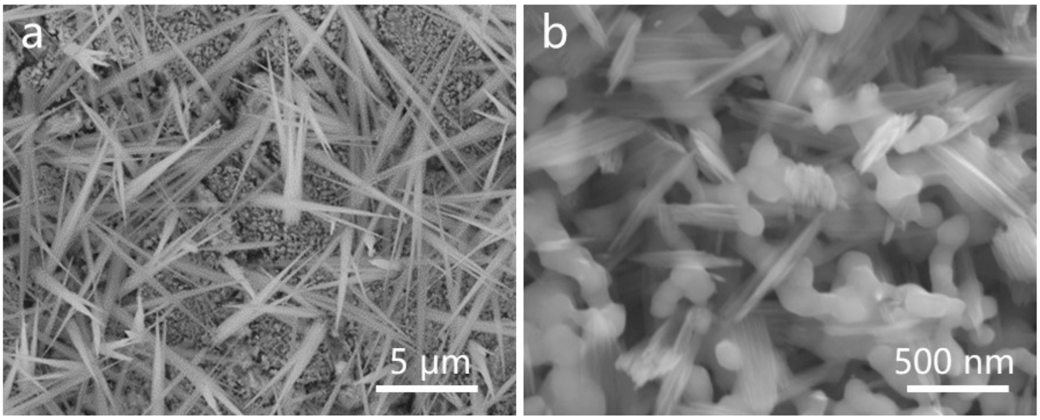

Figure S3. SEM images of (a) the external surface and (b) the cross-section morphologies of NP-CuAg after electrochemical oxidation for 5 minutes.

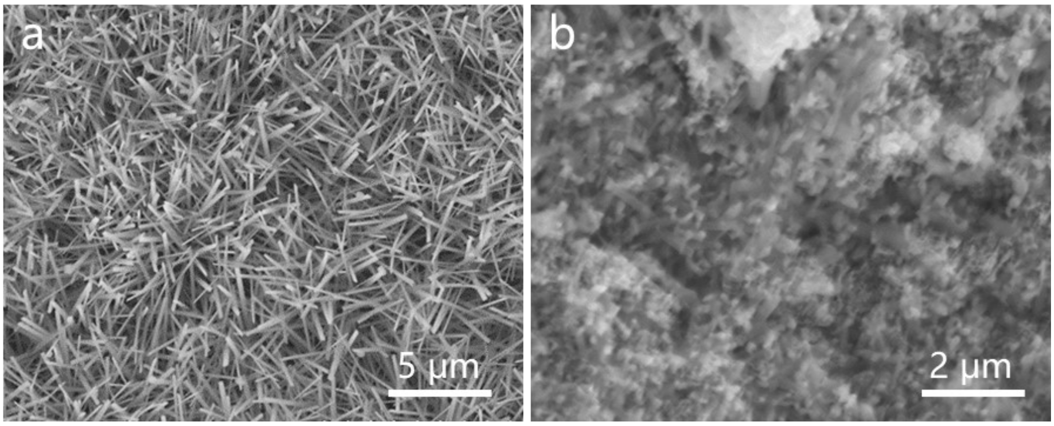

Figure S4. SEM images of (a) the external surface and (b) the cross-section morphologies of NP-CuAg after chemical oxidation for 60 seconds.

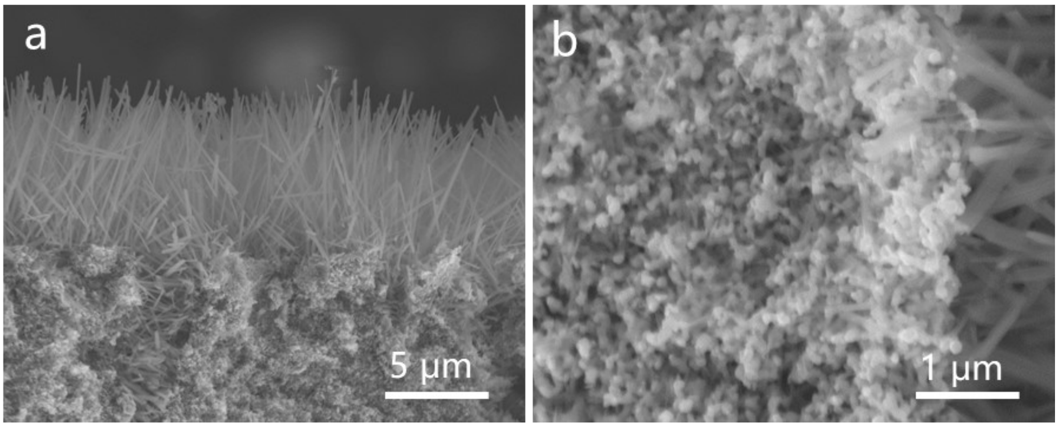

Figure S5. (a) and (b) SEM images showing the hierarchical $Cu(OH)_2$ nanograsses of the NP-CuAg@TSO sample, characterized by large nanograsses on the external surface interspersed with uniformly distributed miniature nanograsses within the porous channels.

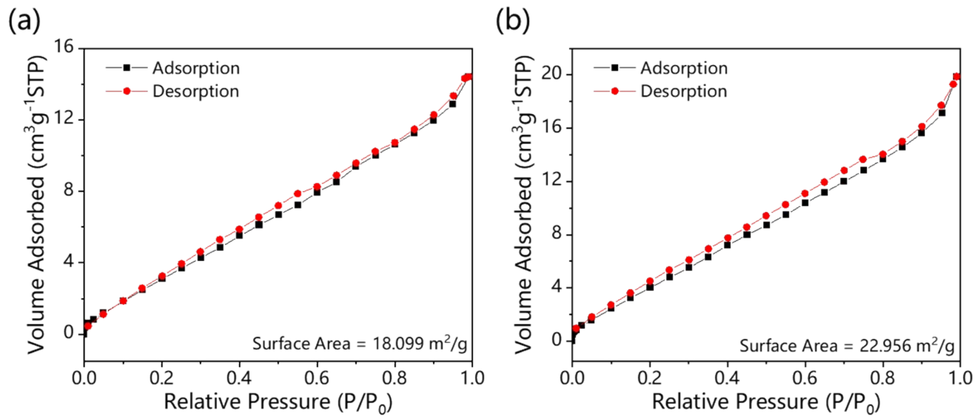

Figure S6. N_2 adsorption and desorption isotherms and specific surface area measurements for (a) NP-CuAg@CO and (b) NP-CuAg@TSO.

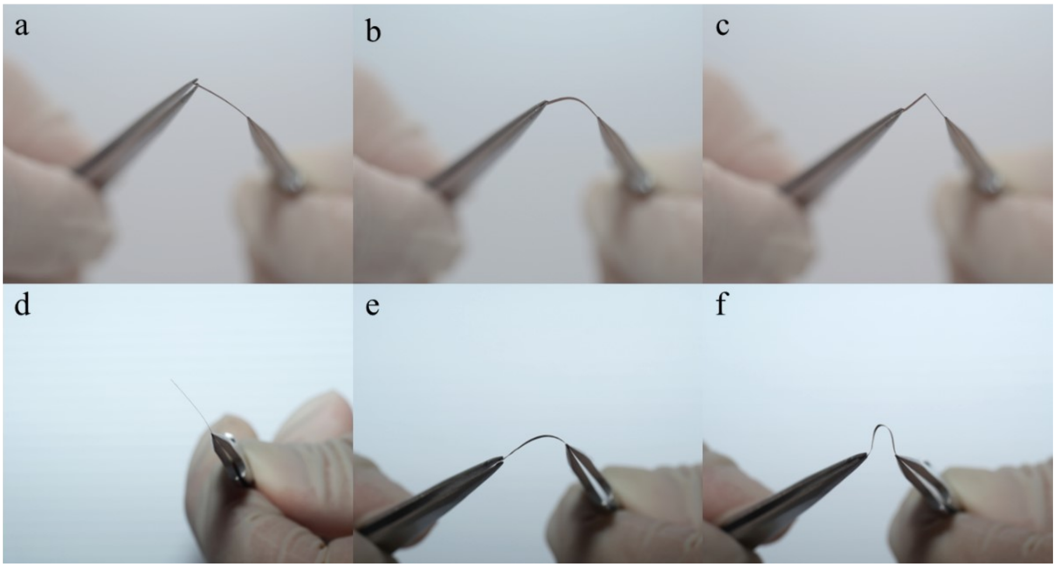

Figure S7. Photographs of (a-c) the AP-CuAg and (d-f) NP-CuAg@TSO during simple bending tests.

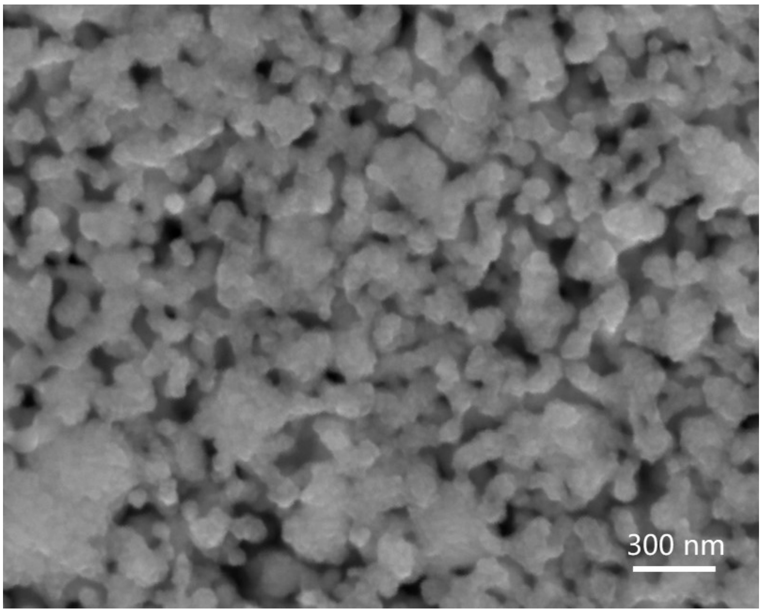

Figure S8. The cross-section SEM image of NP-Cu.

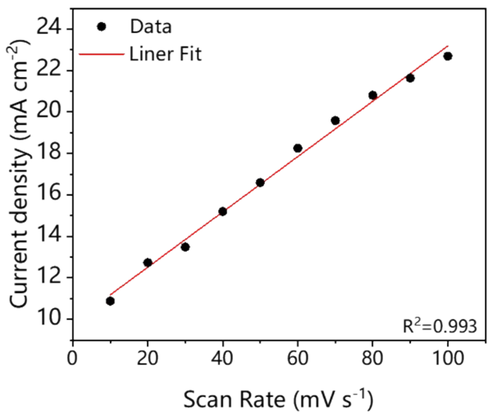

Figure S9. Plot of the linear fit of the oxidation peak current at different scan rates.

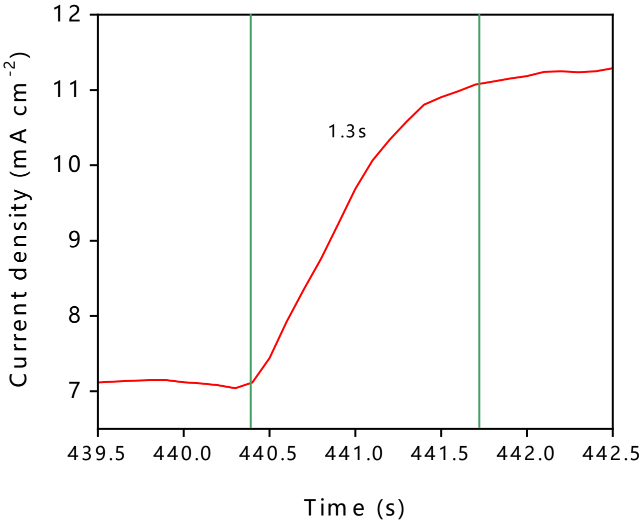

Figure S10. Current response time of the NP-CuAg@TSO.

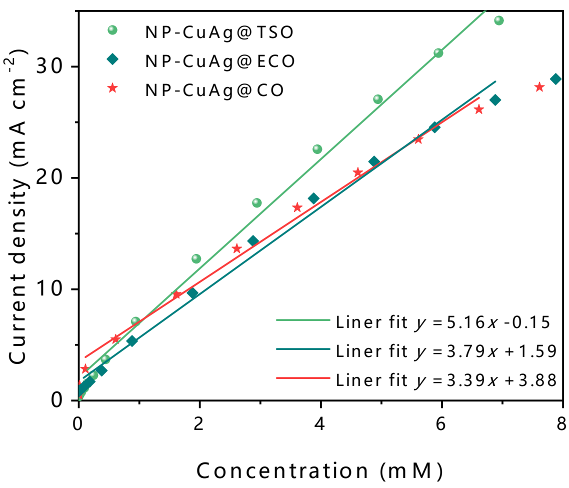

Figure S11. Linear fitting of the current response curve of the NP-CuAg@TSO, NP-CuAg@ECO, and NP-CuAg@CO and sensitivity values.

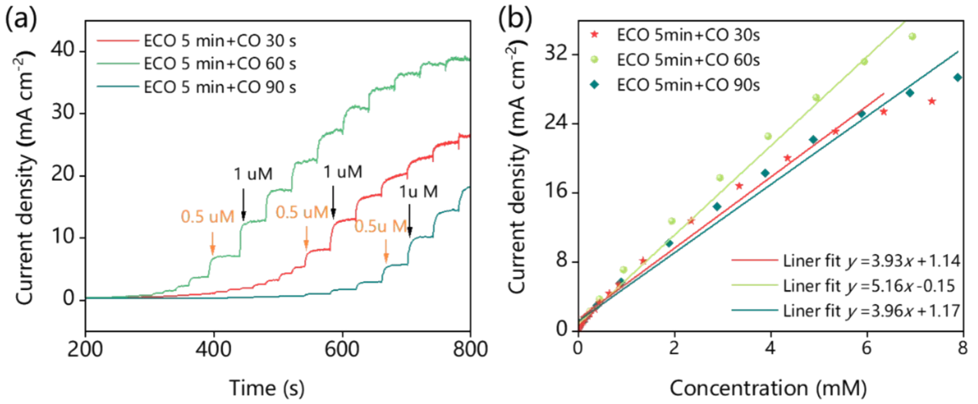

Figure S12. Plots of (a) current response curves of electrodes with different oxidation times for different concentrations of glucose and (b) corresponding linear fit and sensitivity values.

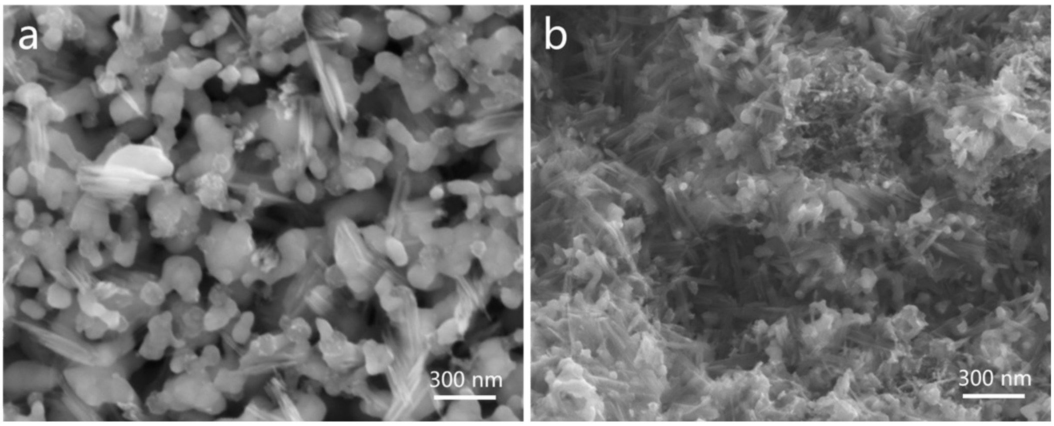

Figure S13. SEM images of the cross-section morphologies of NP-CuAg after electrochemical oxidation for (a) 30 seconds and (b) 120 seconds.

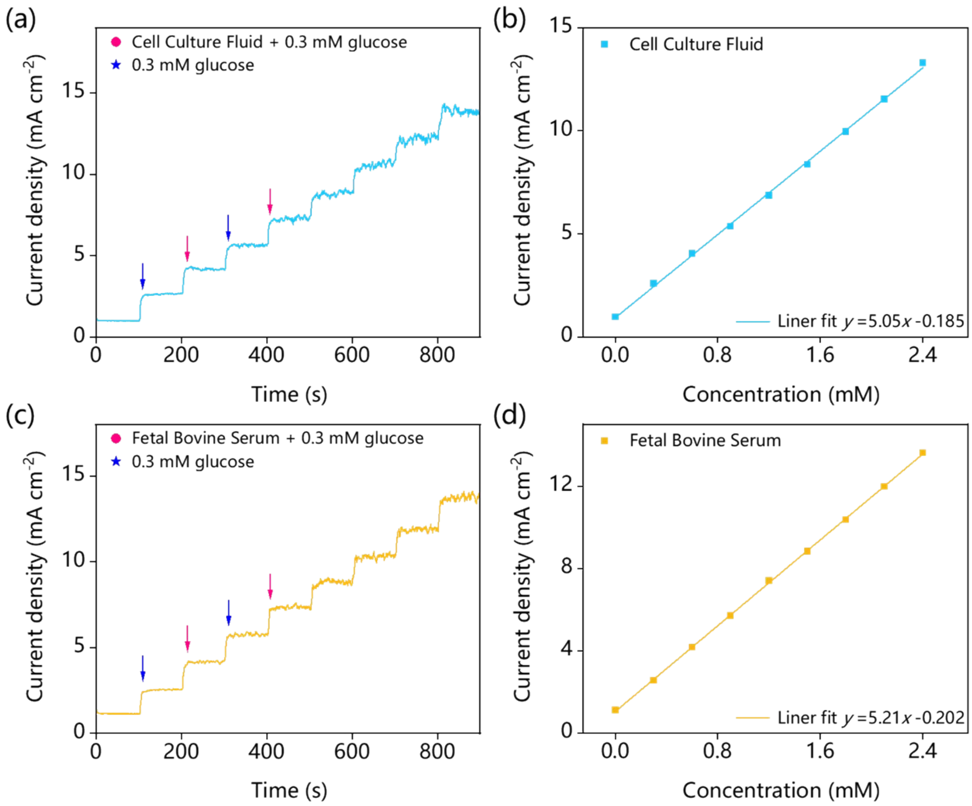

Figure S14. The current response curves of alternating injection of 0.3 mM glucose and simulated real samples (such as cell culture medium (a) and fetal bovine serum (c)). The linear fitting graph (b and d) between current and glucose concentration from Figure S14a and c, respectively.

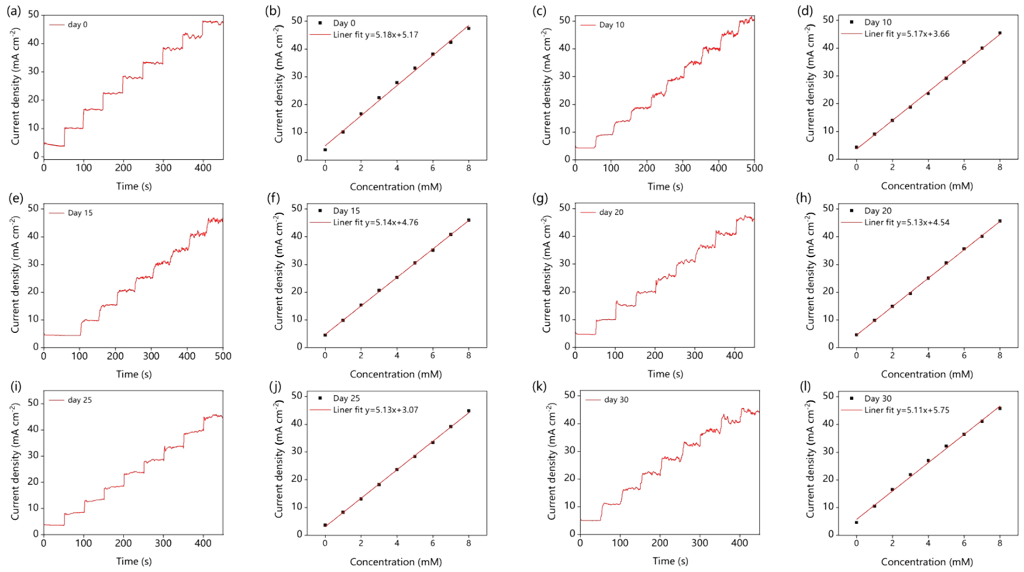

Figure S15. The *i-t* response curves and corresponding evaluation of sensitivity with intervals of several days.

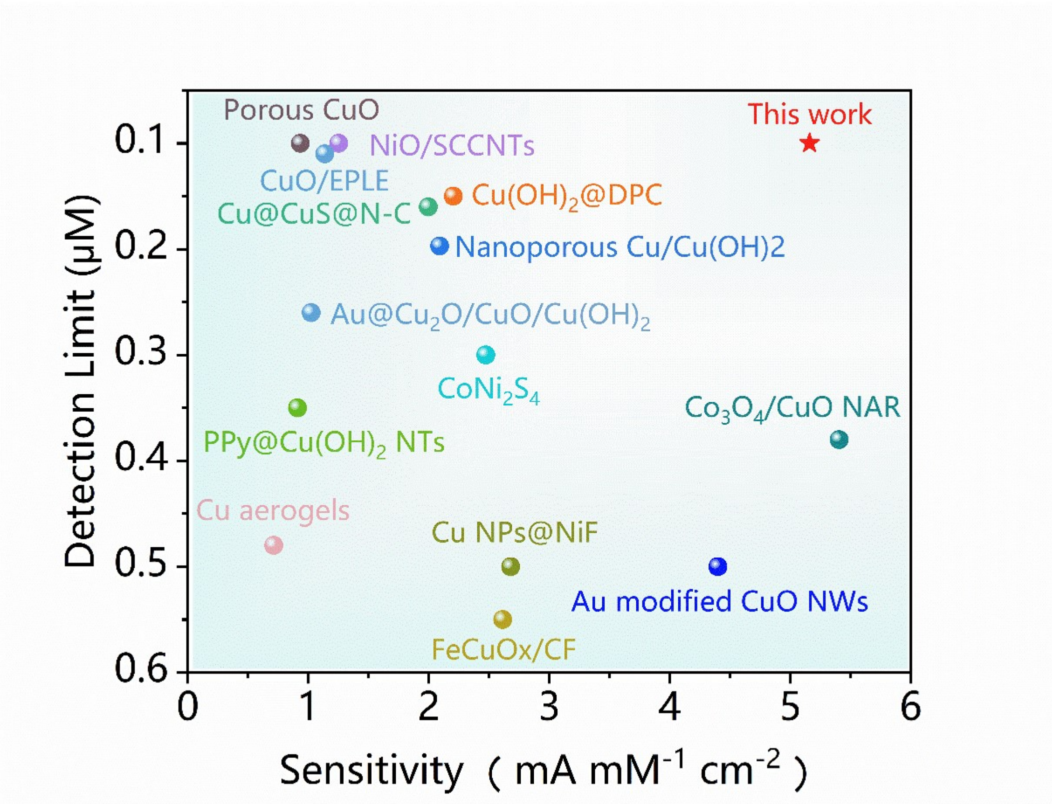

Figure S16. Comparison of glucose oxidation performance of other electrodes for glucose sensing.[1-13]

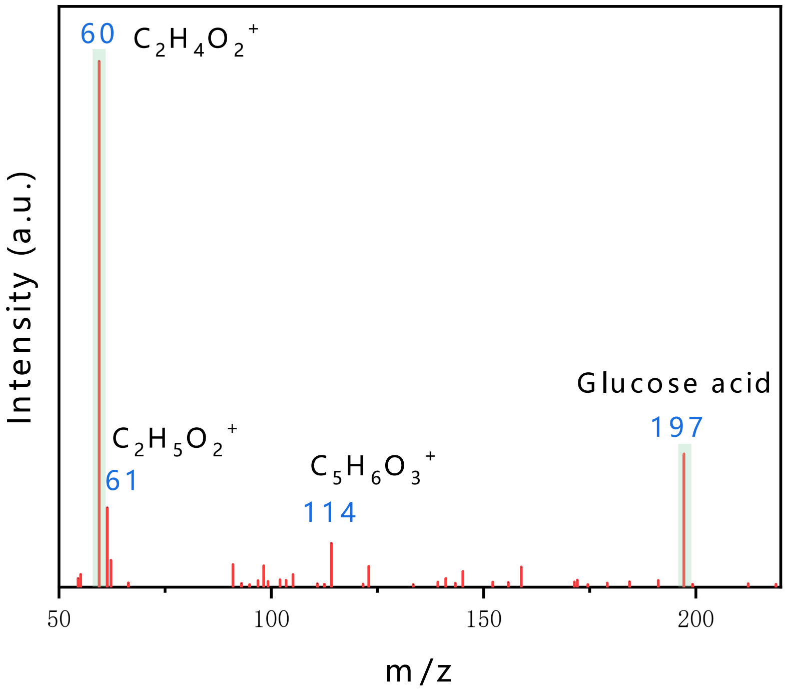

Figure S17. Liquid chromatography-mass spectrometer results of electrooxidation product of glucose.

Table S1. The equivalent circuit fitting parameters for impedance of each sample.

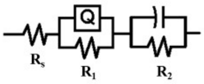	NP-Cu	NP-CuAg	NP-CuAg @CO	NP-CuAg @ECO	NP-CuAg @TSO
R_s (Ω)	20.54	27.21	23.09	21.9	21.03
R_1 (Ω)	192.6	64.28	70.39	75.74	35.1
CPE_1 (F)	0.00037	0.01509	0.003711	0.009555	0.02285
R_2 (Ω)	2556	136.7	143	204.8	110.4
CPE_2 (F)	0.00027	0.04729	0.002293	0.04576	0.07803

References

1. L. Li, Y. Liu, L. Ai, J. Jiang, *Ind. Eng. Chem.*, 2019, 70, 330-3372.
2. M.H. Raza, K. Movlaee, Y. Wu, S.M. EI-Refaei, M. Karg, S.G. Leonardi, G. Neri, N. Pinna, *ChemElectroChem*, 2019, 6, 383–392.
3. X. Yu, J. He, S. Du, Z. Xu, S. Sun, Y. Tang, K. Zhao, *New J. Chem.*, 2023, 37, 17267-17276.
4. Q. Fang, H. Wang, X. Wei, Y. Tang, X. Luo, W. Xu, L. Hu, W. Gu, C. Zhu, *Adv. Healthc. Mater.*, 2023, 12, 2301073.
5. A.K. Mishra, B. Mukherjee, A. Kumar, D.K. Jarwal, S. Ratan, C. Kumar, S. Jit, *RSC Adv.*, 2019, 9, 1772-1781.
6. S. Cheng, S. DelaCruz, C. Chen, Z. Tang, T. Shi, C. Carraro, R. Maboudian, *Sensor Actuat. B-Chem.*, 2019, 298, 126860.
7. M. Reza, S. Saeed, H.K. Mohammad, *Microchem. J.*, 2021, 169, 106636.
8. Y. Ao, J. Ao, L. Zhao, L. Hu, F. Qu, B. Guo, X. Liu, *Langmuir*, 2022, 38, 13659–13667.
9. Y. Xu, J. Zhao, L. Qin, X. Tang, B. Wu, Y. Xiang, *Sens. Actuators. Rep.*, 2022, 4, 100090.
10. R. Li, X. Liu, H. Wang, Y. Wu, Z. Lu, *Biosens. Bioelectron.*, 2018, 102, 288-295.
11. P. Ma, X. Ma, Q. Suo, F. Chen, *Sensor Actuat. B-Chem.*, 2019, 292, 203-209.
12. X. Yang, P. Jiao, G. Zhu, Y. Zeng, Q. Wang, G. Qiu, C. Wang, H. Yu, *Colloids and Surfaces A.*, 2024, 703, 135301.
13. L. Yu, M. Lv, T. Zhang, Q. Zhou, J. Zhang, X. Weng, Y. Ruan, J. Feng, *Anal. Methods*, 2024, 16, 731-741.